INTERNATIONAL JOURNAL OF
COASTAL, OFFSHORE & ENVIRONMENTAL ENGINEERING IJCOE Vol.7/No. 3/Summer 2022 (31-42)

Available online at: www. Ijcoe.org

Spatial and temporal variations of the electrical conductivity and magnetic field of the Caspian Sea using Princeton Ocean Model

Sobhan Eskandari[1], Dariush Mansoury[2*]

[1] *Graduate of Physical Oceanography Department, Faculty of Natural Resources and Marine Sciences, Tarbiat Modares University; eskandarisobhan@modares.ac.ir*

[2*] *Assistant Professor, Physical Oceanography Department, Faculty of Natural Resources and Marine Sciences, Tarbiat Modares University; mansoury@modares.ac.ir*

ARTICLE INFO

Article History:
Received: 17 Jul. 2022
Accepted: 09 Oct. 2022

Keywords:
Magnetic field anomaly
Electrical conductivity
Electromagnetic induction
POM model
Caspian Sea

ABSTRACT

In this study, changes in the magnetic field and electrical conductivity across the Caspian Sea Basins were investigated using the Princeton Ocean Model (POM). In this model, bathymetry, temperature and salinity and atmospheric flux data were collected from GEBCO08, WOA and ECMWF databases, respectively. This model was implemented for ten years (2009-2019), and temperature, salinity and current velocity were extracted from the model output to calculate the electrical conductivity and simulate the magnetic field anomalies of the Caspian Sea. The calculated electrical conductivity indicates that the dominant factor in electrical conductivity was temperature. In the study area, the highest and lowest electrical conductivity were in the southern Caspian basin (SCB) with a value of 2.3 S/m in summer and in the northern Caspian basin (NCB) about 0.8 S/m in autumn. Also, the results show the highest and lowest magnetic fields in the SCB were 16 nT in March and 12 nT in November, respectively. The distribution of magnetic field anomalies with different values in the middle Caspian basin (MCB) can also be observed for all months. According to the results, the dominant factor in the magnetic field anomalies is the current velocity, which has the most effect on the magnetic field in the western part of the Caspian Sea.

1. Introduction

Electro-magnetic induction due to the flow of conducting seawater in the Earth's magnetic field has been a subject of research interest for many years [e.g.: 1, 2, 3, 4, 5, 6]. There has been a recent increase of research activities [e.g.: 7, 8, 9, 10, 11, 12, 13, 14, 15, 16, 17, 18]. The oceans play a special role in this induction due to their relatively high conductivity which leads to large lateral variability in surface conductance. The ocean-induced magnetic field is the smallest component of the Earth's magnetic field, and is five orders weaker than the Earth's magnetic field [18, 20]. These ocean magnetic signals are generated by sea interactions with the Earth's magnetic field. The magnetic field observed near the Earth's surface shows the interference of different magnetic field components [21]. The Earth's core field, known as the main field, generates more than 90% of the geomagnetic field measured at the Earth's surface. The Earth's magnetic field is generated by the movement of conductive material in the liquid part of the Earth's core, called Geodynamo, and refers to the core field. The Earth's surface magnetic field, generated by the Geodynamo core, resembles a dipole in the center of the Earth with a magnetic field ranging from 30,000 nT at the equator to more than 60,000 nT in the polar regions [22]. Another source of magnetic field is ocean dynamics. The oceans produce a magnetic field because the salty sea-water is a conductive fluid with a mean value between 3 to 4 S/m. Electrical signals detectable above the ground are due to seawater movement and ocean circulation caused by winds on the sea surface and differences in density due to changes in temperature and salinity. This combination of magnetic fields is the main subject of this research and is discussed in more detail. The studies show that the change in the electrical conductivity of seawater affects the characteristics of increasing and decreasing electromagnetic fields [23]. The electrical conductivity of the seawater in turn is mainly dependent on seawater temperature and salinity distribution [24]. which can be estimated using the Apel (1987) approximation [25], where temperature is

the dominant component [26]. The seawater electrical conductivity can be considered constant or variable with time; often variable electrical conductivity is considered instead of constant electrical conductivity distribution in the ocean [27]. As the oceans pass through the Earth's main magnetic field, the ionic content in the oceans generates electrical currents which flow across the world's oceans and produce magnetic fields called secondary magnetic fields. Electric currents that generate secondary fields are induced in the oceans by two different processes: (a) by time varying external magnetic fields, and (b) by the motion of the conducting ocean water through the Earth's main magnetic field [19]. An important question to be answered by such studies is whether the magnitude of the ocean induced magnetic field, (b), is sufficient for detection by present magnetometers. Magnetic field measurements at the ocean showed that this amount reached several nanotesla. In situ measurements at and below the ocean surface demonstrated that this magnitude reaches many tens of nanotesla [28]. Ocean eddies near Tasmania induce up to 25-nT magnetic fields at the sea surface. However, present numerical models predict much lower values. Stephenson and Bryan (1992) found the vertical component, bz, of the field at the sea surface to be of order 1 nT, while Tyler et al. (1997) and Vivier et al. (2004) reported field magnitudes within a few nanotesla. At the sea surface, in several spots south of Australia, at the satellite altitude its maximum value is 6 nT, also much larger than in the earlier studies. Similar calculations using ocean data products from the 1 °-resolution version of the ECCO-MIT model yield 20 nT as the maximum amplitude of the surface field, and 4 nT at 430 km [29]. Tyler et al. (1997) obtained the anomalies of the magnetic field in Antarctica and concluded that the changes in the magnetic field were about 2 nT at a depth of 20 m, 10 nT at a depth of 100 m, and up to several tens of nanotesla at lower depths. Researchers are interested in understanding the magnetic field produced by the ocean for a number of reasons. First, the ocean's magnetic field has become interesting for many oceanographers to study more about ocean currents. Secondly, the ocean's magnetic field is also relevant to geophysicists studying geological structures under the ocean [4]. However, the detection of the presented signals in satellite-based magnetometer measurements may be challenging today [30]. Nonetheless, the precision of the observations might improve with longer observation time series, by future processing improvements or through future magnetometer satellite missions. In addition, terrestrial magnetometers should be used. The expected changes at sea level (or ocean bottom) are of the order of several 0.1 nT and should be detectable by magnetometers on land, at ocean bottom, by deep sea telecommunication cables or in induction-based Tsunami early warning networks [31, 32, 33, 34]. The electrical conductivity of seawater samples on the southern shores of the Caspian Sea was measured at about 23 dS/m [35]. So far, no research has been done on the magnitude of the magnetic field in the Caspian Sea basins. In this research, for the first time, in a 0.08 °-resolution version of the POM model, oceanographic parameters such as temperature, salinity and current velocity were extracted and then they were used as inputs to study changes in magnetic field and electrical conductivity in the three Caspian basins. Tidal motions are not included in this analysis, because the tides in the Caspian Sea are negligible.

2. Methodology

2.1. Study area

The Caspian Sea is the largest lake in the world. All the features of the Caspian Sea, including size, depth, chemical properties, as well as circulation and thermohaline properties, classify it as a deep inland sea. In 2016, the average level of the Caspian Sea was measured to be -27.43 m against the surface of the Atlantic Ocean [36]. The Caspian Sea has a longitudinal geometry (1000 km long and 200 to 300 km wide) and has three northern, middle, and southern basins (Figure 1). The maximum depth in the northern basin is 20 m while the maximum depths in the middle and southern basins are 788 m and 1025 m, respectively [37]. Sea surface temperature in the NCB reaches below zero in winter and 25-26 °C in summer. In the southern Caspian basin (SCB), it occurs from 7-10 °C in winter to 25-29 °C in summer. The Caspian Sea has little salinity. In the deepest region, salinity changes reach about 12 psu to 13.5 psu [38, 39]. The elongated geometry and specific topography in the Caspian basins, acted upon by variable wind forcing and baroclinic effects result in spatially and temporally variable currents in the Caspian Sea. Despite strong variability of the sea currents, the general circulation has been described to be cyclonic. Especially standing out among these were the six instrumental surveys along the western coast of the MCB, carried out in the years 1935–1937 [40], showing predominantly southward currents along the western coast of the MCB, modified by wind-driven currents close to the surface [37, 41].

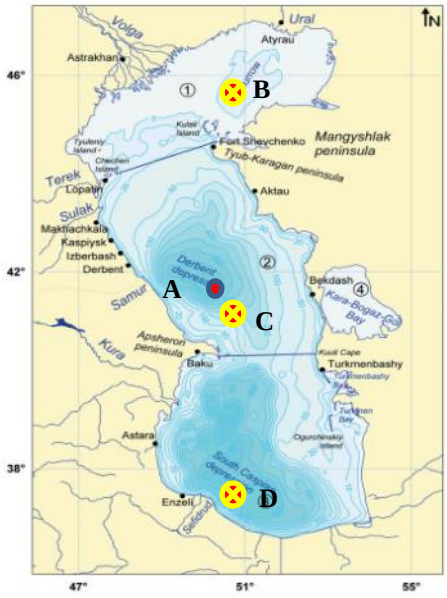

Figure 1. Caspian Sea [34]

2.2. Numerical system

The Princeton Ocean Model (POM) is a numerical ocean model on sigma coordinates, a right-angled curved horizontal grid, free surface boundary conditions, as well as turbulence and wave sub-models. It can be used for a wide range of issues such as circulation and mixing process in rivers, estuaries, continental shelf and slope, lakes, semi-closed and open oceans [42]. It uses the Mellor and Yamada (1982) turbulence closure scheme [43], while the horizontal viscosity terms are provided by the Smagorinsky (1993) parameterization [44]. Numerous applications of this model in the modeling field in oceans and seas have been studied in different parts of the world by many international researchers [45, 46, 47]. Message passing interface Princeton Ocean Model (mpiPOM) was developed by Advanced Taiwan Ocean prediction (ATOP) and is optimized for the needs and resources of the ATOP system [48]. It is desirable in terms of computer economy to separate vertically integrated equations (external mode) from vertical structure equations (internal mode). This technique, known as mode splitting [49], permits the calculation of the free surface elevation with little sacrifice in computational time by solving the velocity transport separately from the three-dimensional calculation of the velocity and thermodynamic properties. It generally uses the Smagorinsky diffusivity formula for horizontal diffusion [50]. The numerical technique for solving the temporal part of the equations is based on the mode separation method in which the external and internal modes equations are solved in two and three dimensions, respectively. In this study, the mpiPOM version is used for the Caspian Sea. The model domain is 36.40-47.50 °N and 46.50-55.00 °E with a horizontal resolution of 0.08 ° × 0.08 ° (in co-latitude and longitude) and 35 sigma levels. To apply the parallel processing (mpi), four cores were considered with the computational grid 68 × 52 (Eq. 1).

$$n_{proc} = [(im_{global} - 2)/(im_{local} - 2)] \times [(jm_{global} - 2)/(jm_{local} - 2)] \quad (1)$$

Where im_{global} = x-grid cells for modeled domain, jm_{global} = y-grid cells for modeled domain, im_{local} = x-grid cells for each processor, jm_{local} = y-grid cells for each processor, and n_{proc} =processors (i.e. num_of_nodes). The external time step is set to 5 s and the internal to 150 s. Surface fluxes use the 6-hourly atmospheric analyses from the European Centre for Medium-range Weather Forecast (ECMWF) at 0.125 °-resolution. The parameters used are 10 m winds, precipitation, evaporation, heat flux, and short and long wave radiation. Also, temperature and salinity data are used from World Ocean Atlas (WOA2005) at 1 °-resolution, and bathymetry data from General Bathymetric Chart of the Oceans (GEBCO08) at 0.5 °-resolution. The monthly average of Naval Research Laboratory (NRL) data was used for the data of the rivers (Volga, Kura and Ural) [51]. The model was run for 10 years from 2009 to 2019. After spinning up of 10 years, the model outputs were saved daily. In this study, we analyzed a year (2018) of model outputs. Salinity, temperature and current profiles have been extracted from model outputs. They were finally used to calculate the electrical conductivity into different layers of the Caspian Sea.

2.3. Stability and validation of the model

To check the stability of the model, salinity changes over time are shown in Figure 2a, which shows good stability after seven years of model implementation. To validate the output of the model, according to the measurement data available in 1996 [52], this model was implemented for ten years, from 1988 to 1997 [53]. Comparison of model output and in situ measurement data show that they are in good agreement. (Figure 2b). The comparison station is located at 41.5 °N and 50 °E (Figure 1_A).

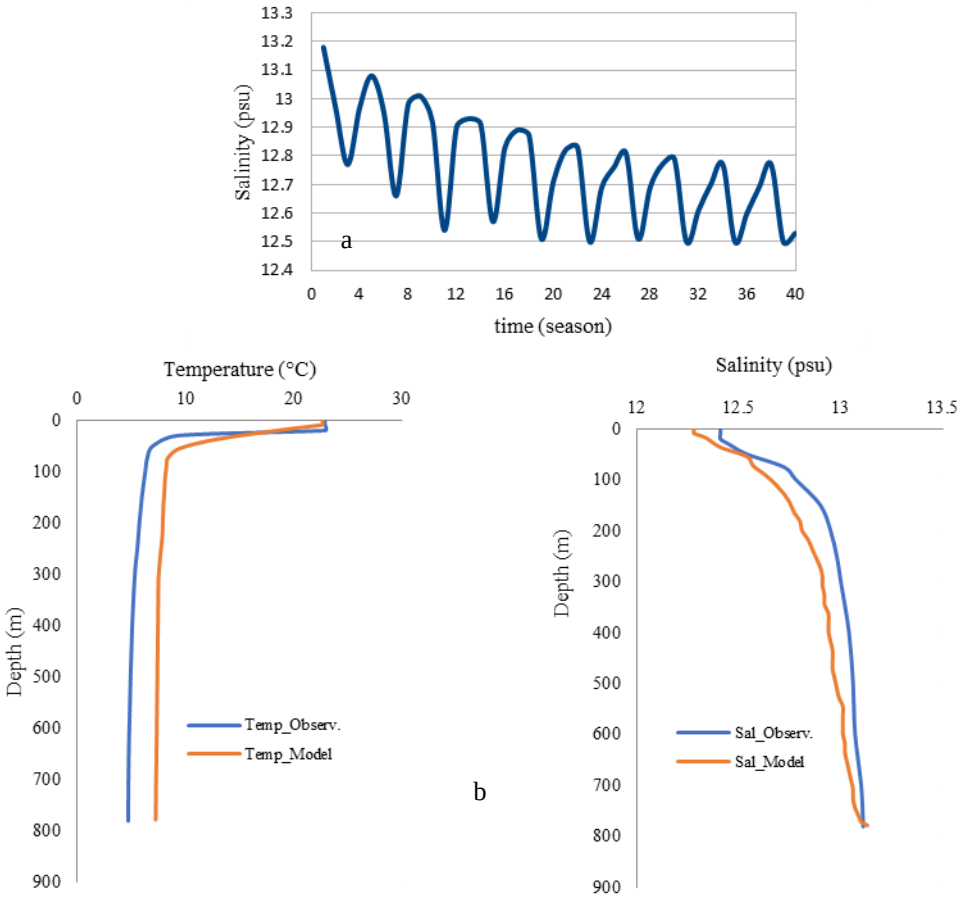

Figure 2. Stability (a) and validation (b) of the model

2.4. Electrical conductivity and Magnetic Field

To investigate the temporal and spatial distribution of electrical conductivity, using the salinity and temperature values extracted from the POM output, the electrical conductivity can be estimated using the method described by Apel (1987; Eqs. 2-5).

$$\sigma(T,s) = \sigma(25,s)\, exp(-\beta\Delta) \quad (2)$$

$$\Delta = 25 - T \quad (3)$$

$$\beta(\Delta,s) = 2.033\times10^{-2} - 1.266\times10^{-4}\Delta + 2.464\times10^{-6}\Delta^2 - s(1.849\times10^{-5} - 2.551\times0^{-7}\Delta + 2.551\times10^{-8}\Delta^2) \quad (4)$$

$$\sigma(25,s) = s(0.182521 - 1.46192\times10^{-3}s + 2.09324\times10^{-5}s^2 - 1.28205\times10^{-7}s^3) \quad (5)$$

Where σ is the conductivity of seawater.

The computation of electromagnetic induction is based on the equations of electromagnetic induction by Maxwell in 1865 for a moving medium.

a) Ampere's law $\nabla\times\vec{B} = \mu_0\vec{j}$ (6)

b) Maxwell- Faraday's law $\nabla\times\vec{E} = -\frac{\partial\vec{B}}{\partial t}$ (7)

c) Gauss's law $\nabla\cdot\vec{B} = 0$ (8)

Where $\vec{B}$ is the main magnetic field, $\vec{E}$ is the electric field, $\vec{j}$ is the electric current density, and μ_0 is the vacuum permeability coefficient. In addition, the generation of electric currents due to a moving conductor with the presence of electric and magnetic fields is described by Ohm's law.

$$\vec{j} = \sigma(\vec{E} + \vec{u}\times\vec{B}) \quad (9)$$

Where σ is the seawater electrical conductivity and $\vec{u}$ is the velocity of seawater. By applying the Ohm's law to the Maxwell-Faraday law, the equation (10) is obtained, and also, the general equation of electromagnetic induction (Eq. 11) is derived from the combination of the equations (6)-(10):

$$\nabla\times(\frac{\vec{j}}{\sigma} - \vec{u}\times\vec{B}) = -\frac{\partial\vec{B}}{\partial t} \quad (10)$$

$$\frac{1}{\mu_0}\nabla\times(\frac{1}{\sigma}\nabla\times\vec{B}) - \nabla\times(\vec{u}\times\vec{B}) = -\frac{\partial\vec{B}}{\partial t} \quad (11)$$

The maximum error for temperature for depths less than and more than 50 meters is about 5% and 12%, respectively, and also the maximum error for salinity is about 17% (at a depth of about 200 meters), but the average errors for temperature and salinity is less than 10%. As the comparison of the results show, there is a good agreement between the annual mean of the SST satellite image (Figure 3a) and the findings of the present study (Figure 3b).

2.5. Thin-Shell Approximation

The physical model which will be the basis of our calculations is that of a spherical shell whose outer radius is the surface of the oceans and whose inner radius corresponds to the maximum depth of the oceans.

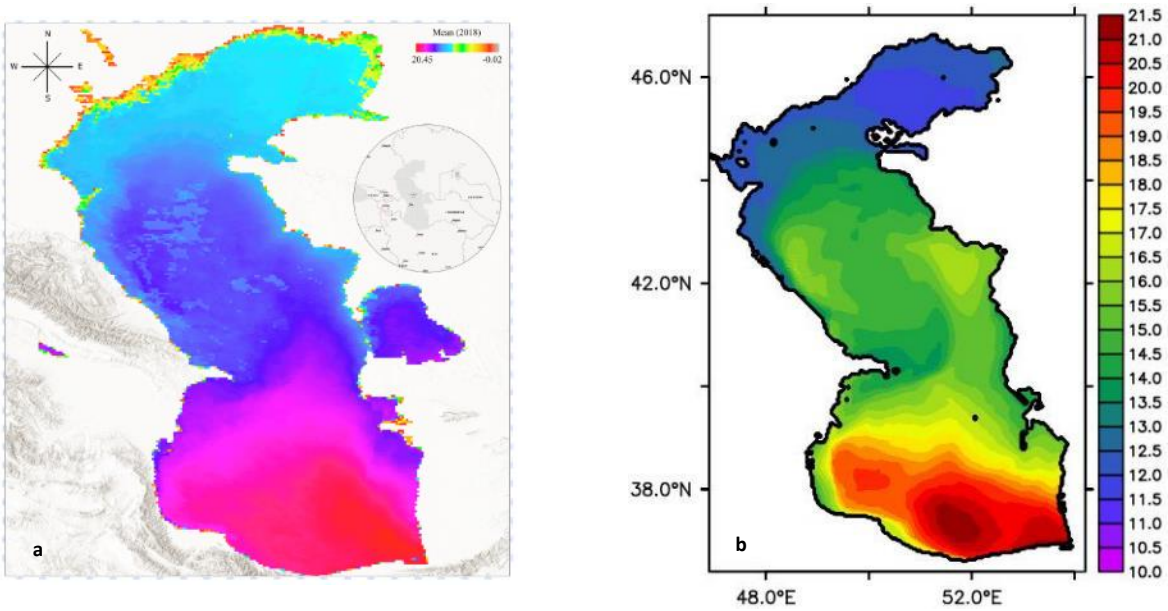

Figure 3. Annual mean climatic field of the SST (°C) a) Satellite image (https://oceancolor.gsfc.nasa.gov/) b) Model output in the Caspian Sea

Therefore, the atmosphere above the shell and the crust below the shell are perfect insulators, a good approximation known as a complete insulator [2]. The conductivity of seawater depends on both temperature and salinity and this may play a role in the variability of the oceanic magnetic and electric fields. The full magnetic field is divided into two parts (see Eq. 12), Earth's main magnetic field due to electric currents in the Earth's core ($\vec{F}$), of which only the radial component Fz is important, and the secondary magnetic field ($\vec{b}$) is the magnetic field induced by electric currents generated in the ocean's velocity [4, 29].

$$\vec{B} = \vec{F} + \vec{b} \quad (12)$$

It will not consider domains including the Earth's core so the source currents for $\vec{F}$ are zero in the region where (Eq. 11) is to be solved. Therefore:

$$\nabla \times \vec{F} = 0 \quad (13)$$

Assuming the environment is quasi-static, the electric field $\vec{E}$ can be written as a potential scalar gradient. The characteristic magnitude of the magnetic field at the sea surface is estimated as the equations (14, 15) [29]:

$$b = \mu_0 F_z S \quad (14)$$

$$S = \int_{-h}^{0} \sigma u_H dz \quad (15)$$

Where u_H is the horizontal velocity and S is the electric conductivity flux. In order to compute σ(z) and S we used vertical profiles of ocean current velocities observed at two locations and climatological data on ocean temperature and salinity.

2.6. IGRF Magnetic field model

The International Geomagnetic Reference Field (IGRF) is an established numerical model used to calculate the large scale, internal part of the Earth's magnetic field at times between 1900.0 A.D. and present, at locations on or above Earth's surface [54, 55, 56]. It is produced and maintained by a team of geomagnetic field modelers under the auspices of the International Association of Geomagnetism and Aeronomy (IAGA) Working Group V-MOD and is derived from observations collected by satellites, at magnetic observatories, and during magnetic surveys. It is used by scientists (e.g. in studies of space weather or in investigations of local magnetic anomalies) and also by commercial organizations and private individuals who often use the geomagnetic field as a source of orientation information. The IGRF model is reviewed every 5 years to be as accurate as possible [57]. To derive the radial component of the Earth's geomagnetic field, we used the IGRF magnetic field model. In this study, the IGRF model has been configured by a spatial resolution of 0.16˚ for 36.40-47.50 °N and 46.50-55.00 °E. The vertical geomagnetic component (F_z) data are extracted as the monthly mean for 2018.

3. Result and Discussion

3.1. Surface Electrical Conductivity

In this study, after spinning up of 10 years (2009-2019) and using the model outputs (temperature, salinity fields and currents), changes in magnetic field and electrical conductivity were studied in the Caspian Sea. The spatial and temporal distribution of electrical conductivity indicates that electrical conductivity has varied at different geographical locations.

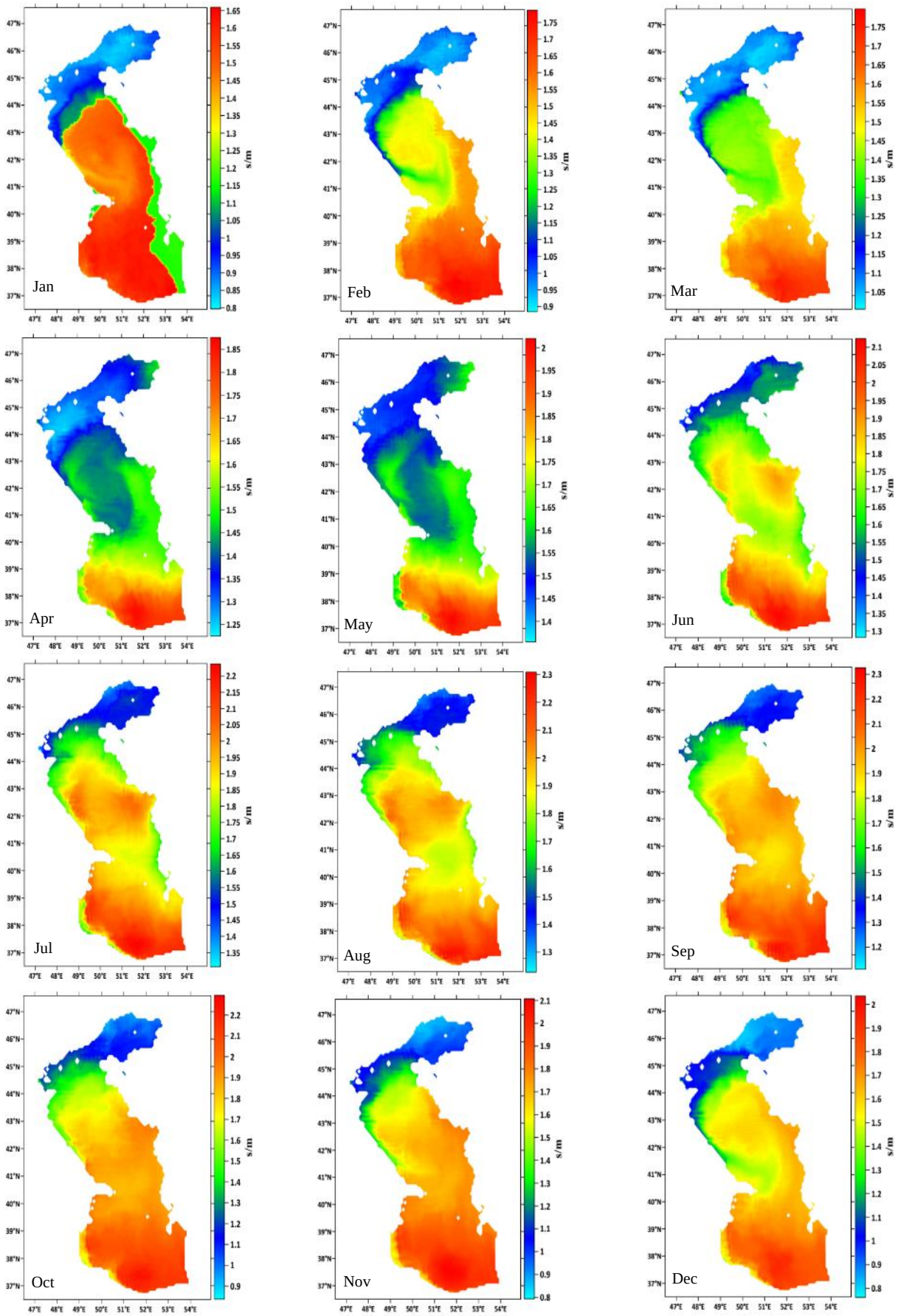

Figure 4. Monthly changes in electrical conductivity in the Caspian Sea

Figure 4 shows the monthly surface distribution of electrical conductivity in the Caspian Sea. In winter, the lowest electrical conductivity was observed in January with a value of 1.65 S/m and the highest electrical conductivity was observed in March with a value of more than 1.75 S/m. In

this season, the maximum electrical conductivity is in the SCB. In spring, the electrical conductivity increased compared to winter, with the electrical conductivity of 1.85 S/m and 1.2 S/m in April and June, respectively. The electrical conductivity changes in April and May were approximately similar in the middle and southern Caspian basins, but it increased in the MCB in June (Figure 4). In summer, due to increasing temperature, more electrical conduction changes are observed than in other seasons. In this season, the highest electrical conductivity (2.3 S/m) was observed in the SCB. In autumn, as shown in Figure 4, due to the decreasing temperature compared to summer, the electrical conductivity decreased in the NCB from 0.9 S/m in October to 0.8 S/m in November and December (Figure 4). Similarly, the electrical conductivity in the SCB also decreased according to the results, so that in December, the electrical conductivity reached 2 S/m.

3.2. Structure of vertical electric conductivity

For a more detailed study of the electrical conductivity, the vertical structure of the electrical conductivity from the sea surface to seabed was calculated for three positions B (45.79℃*N*, 50.71℃*E*; 7m depth), C (41.12℃*N*, 50.71℃*E*; 235m depth) and D (37.37℃*N*, 50.71℃*E*; 735m depth) (see Figure 1a) in February and July. The results of the analysis in the three basins show that in the SCB, there are relatively intense changes in electrical conductivity from the surface to a depth of 300 meters (Figure 5). In February, in this basin, the electrical conductivity and temperature decreased to a depth of about 70 meters (thermocline layer) and then it increased to a depth of 300 meters, due to the constant temperature and in proportion to the increasing changes in salinity, and from 300 m up to the seabed, similarities in temperature and salinity are almost unchanged. In July, the electrical conductivity and temperature decreased to a depth of about 100 meters (thermocline layer) and then is almost unchanged up to the seabed. As a result, electrical conductivity changes in the cold season are affected by changes in temperature and salinity, but in the hot season it is mainly affected by temperature changes.

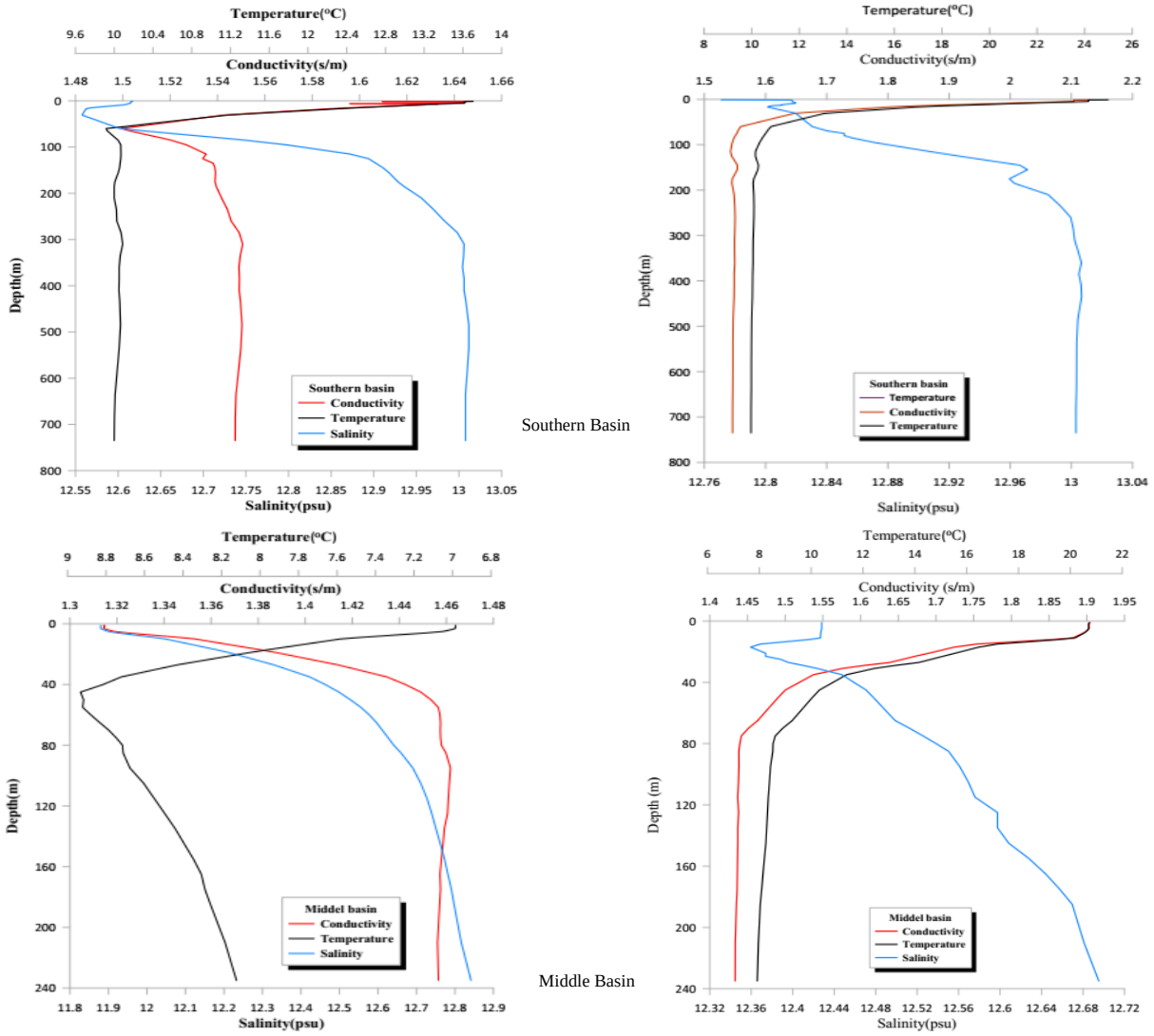

Figure 5. The electrical Conductivity, Temperature and Salinity Profiles in February (Left) and July (Right)

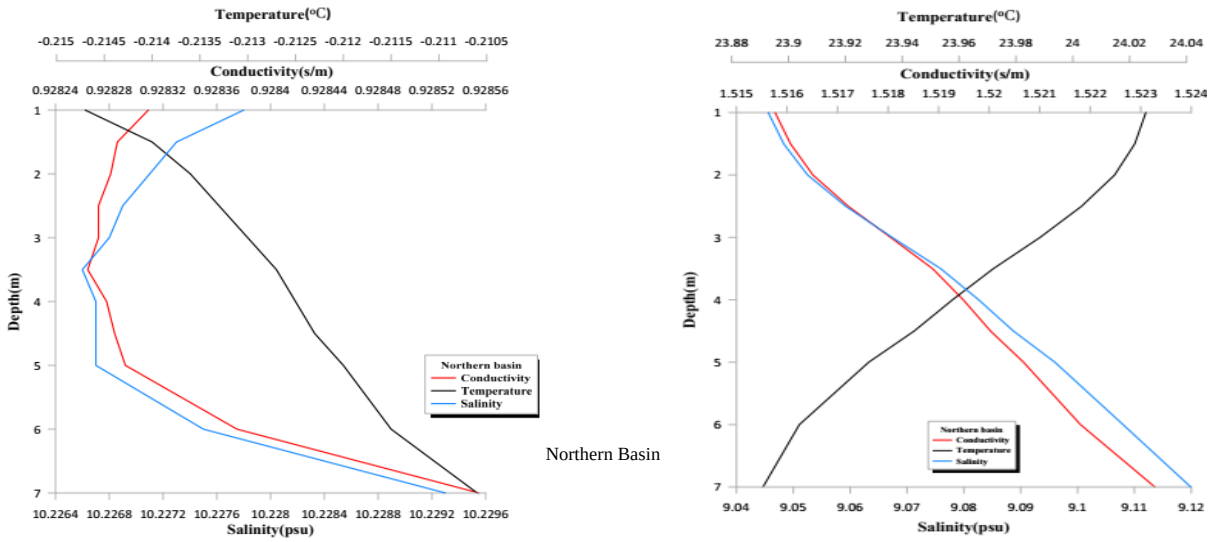

Figure 5. Continue

According to Figure 5. the electrical conductivity profiles in the MCB show that in February, electrical conductivity changes from the surface to the seabed are increasing due to small changes in temperature, according to the increasing changes in salinity. But in July, they are reduced due to large changes in temperature and according to the trend of temperature changes. Also, the dependence of electrical conductivity on salinity in the NCB is greater than temperature. In this basin, salinity changes are greater than temperature changes due to the Volga River and shallow water. As a result, the electrical conductivity has changed according to the trend of salinity changes. In February, electrical conductivity and salinity decreased to a depth of 3.5 meters and then increased with increasing depth to the seabed. In July, the electrical conductivity changes are increasing, according to the trend of salinity changes.

3.3. Monthly changes of magnetic field

According to equations (6)-(15), the monthly temporal and spatial changes of the magnetic field in the northern, central and southern Caspian basins for 2018 have been studied (Figure 6). The monthly changes of the magnetic field in most of the Caspian Sea are less than 1 nT (of the order of 0.1 nT). Its average value in some deep regions is about 3 and 6 nT in the middle and southern basins of the Caspian Sea, respectively. The highest magnetic field is in the SCB. The magnetic field anomaly in the Caspian Sea is more intense in the southern basin in winter. In spring, the magnetic field anomalies reduced compared to winter in the MCB and NCB. In the spring, magnetic field anomalies are reduced in the MCB and NCB compared to the winter. This decrease in magnetic field is more intense in MCB than in NCB. In summer, the magnitude of the magnetic field in the MCB was much lower than winter and spring, about 1 nT - 2 nT in August. In autumn, the magnetic field intensely increased in the MCB (about 5 nT. The results show that in all months the highest magnetic field anomaly occurred in the SCB, so that in March, a magnetic field of up to 16 nT was observed in the SCB.

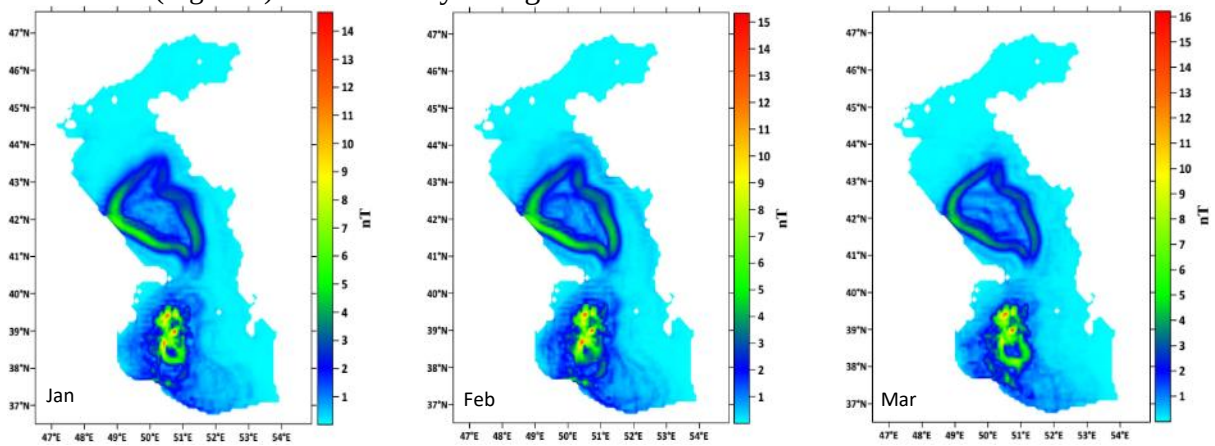

Figure 6. Monthly changes of Magnetic field in the Caspian Sea

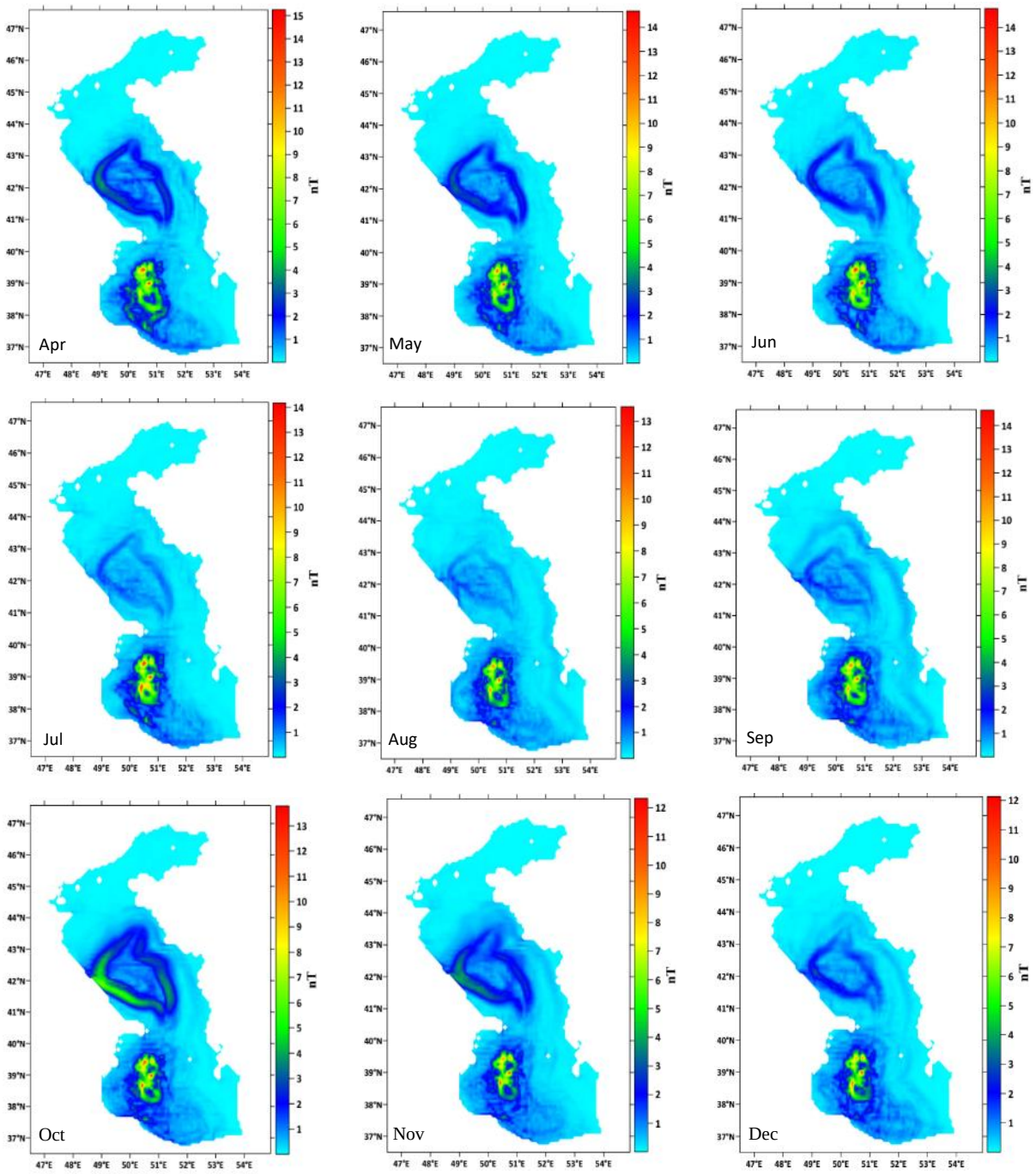

Figure 6. Continue

It shows the lowest magnitude of magnetic field anomalies in October and November with a value of approximately 12 nT in the SCB. But the highest magnetic field changes are observed in the MCB in all months. The magnetic field anomaly is a function of the electrical conductivity flux and current velocity. To calculate the magnetic field anomaly using the sum of layers of electrical conductivity flux $\int_{-h}^{0} \sigma u_H dz$ from surface $z = 0$ to depth $z = -h$, it can be concluded that the maximum magnetic field anomaly obtained in the Caspian Sea is a function of depth and sea current.

4. Conclusion

The Princeton Ocean Model was used to determine the parameters required to simulate magnetic fields in the Caspian Sea. This combination makes it unique to not only calculate the induced magnetic signals but also to evaluate the influence of oceanographic factors on the magnetic induction process. The electrical conductivity distribution of the SCB showed that the lowest and the highest of surface electrical conductivity were 1.65 S/m in January and 2.3 S/m in August and September, respectively. These findings were in good agreement with the values measured by Dordipour et al. (2004). In July and February, changes in electrical conductivity, in the SCB and MCB, are

proportional to temperature changes, while in the NCB, it is proportional to changes in salinity. The expected changes at sea level (or ocean bottom) are of the order of several 0.1 nT (Saynisch et al. 2016) which is in good agreement with the magnetic field changes in the NCB, due to the shallow depth. Also, the magnetic field anomalies in the southern and middle basins, due to the deep-water depth, are in relatively good agreement with the magnetic field changes in the Ocean (Glazman and Golubev, 2005; Tyler et al. 1997). The results show that the amount of magnetic field anomalies in the NCB was the lowest due to the shallow depth. The magnetic field anomalies are relatively intense in parts of the southern and middle basins. Spatial and temporal changes in the scattering of the magnetic field in the MCB compared to other basins show that the magnetic field anomaly has temporal and spatial variability and is affected by sea currents. In SCB, the highest and lowest magnetic field anomalies were observed in March 16 nT and November 12 nT, respectively. According to the results, the current velocity and depth are the most important factors in changing the magnetic field in the Caspian Sea, which has the most effect on the magnetic field in the western half of the Caspian Sea. The highest magnetic field anomalies in this study (16 nT) are in relatively good agreement with the magnetic field anomalies in South Australia (20 nT) as well as in parts of Antarctica (10 nT at 100 m depth) (Glazman and Golubev, 2005; Tyler et al. 1997). This discrepancy can be due to differences in the thermohaline structure, current velocity and also the vertical component of the Earth's magnetic field in each of the research areas.

5. Reference

[1] Larsen, J., 1992. Transport and heat flux of the Florida Current at 27 ̊N derived from cross-stream voltages and profiling data: Theory and observations, Philos. Trans. R. Soc. London, Ser. A, 338, 169– 236.

[2] Stephenson, D., Bryan, K., 1992. Large-scale electric and magnetic fields generated by the oceans. Journal of Geophysical Research, Vol, 97, no, C10, pp. 15467-15480.

[3] Chave, A.D., and Luther, D.S., 1990. Low-frequency, motionally induced electromagnetic fields in the ocean, J. Geophys. Res., 95, 7185– 7200.

[4] Tyler, R.H., Mysak, L.A., Oberhuber, J.M., 1997. Electromagnetic fields generated by a three-dimensional global ocean circulation. Journal of Geophysical Research: Oceans, Vol, 102, no, C3, pp. 5531-5551.

[5] Flosadottir, A.H., Larsen, J.C., and Smith, J.T., 1997a. Motional induction in North Atlantic circulation models, J. Geophys. Res., 102, 10,353 –10,372.

[6] Flosadottir, A.H., Larsen, J.C., and Smith, J.T., 1997b. The relation of seafloor voltages to ocean transports in North Atlantic circulation models: Model results and practical considerations for transport monitoring, J. Phys. Oceanogr., 27, 1547– 1565.

[7] Tyler, R.H., Maus, S., and Lu¨hr, H., 2003. Satellite observations of magnetic fields due to ocean tidal flow, Science, 299, 239– 240.

[8] Maus, S., and Kuvshinov, A., 2004. Ocean tidal signals in observatory and satellite magnetic measurements, Geophys. Res. Lett., 31, L15313, https://doi.org/10.1029/2004GL020090.

[9] Vivier, F., Maier-Reimer, E., and Tyler, R.H., 2004. Simulations of magnetic fields generated by the Antarctic Circumpolar Current at satellite altitude: Can geomagnetic measurements be used to monitor the flow? Geophys. Res. Lett., 31, L10306, https://doi.org/10.1029/2004GL019804.

[10] Manoj, C., Kuvshinov, A., Maus, S., and Lühr, H., 2006. Ocean circulation generated magnetic signals. Earth Planets Space, 58(4), 429-437.

[11] Khalilabadi, M.R., and Hassantabar, B.S.H., 2016. Investigation of magnetic field fluctuations due to sea waves in the Strait of Hormuz, Journal of Research on Applied Geophysics, 2(1), 23-34.

[12] Irrgang, C., Saynisch, J., and Thomas, M. 2017. Utilizing oceanic electromagnetic induction to constrain an ocean general circulation model: A data assimilation twin experiment. J. Adv. Model. Earth Syst., 9(3), 1703-1720. https://doi.org/10.1002/2017MS000951.

[13] Khalilabadi, M. R., and Shahmirzaee, H. 2017. Marine Magnetic Data Processing and Extracting Magnetic Anomaly. Hydrophysics, 3(1), 1-10.

[14] Irrgang, C., Saynisch-Wagner, J., Thomas, M, 2018. Depth of origin of ocean-circulation-induced magnetic signals. In Annales Geophysicae, Vol, 36, no, 1, pp. 167-180.

[15] Saynisch, J., Irrgang, C., and Thomas, M., 2018. On the Use of Satellite Altimetry to Detect Ocean Circulation's Magnetic Signals. J. Geophys. Res. Oceans, 123(3), 2305-2314. https://doi.org/10.1002/2017JC013742.

[16] Velímský, J., Šachl, L., Martinec, Z., 2019. The global toroidal magnetic field generated in the Earth's oceans. Earth and Planetary Science Letters, Vol, 509, pp. 47-54.

[17] Šachl, L., Martinec, Z., Velímský, J., Irrgang, C., Petereit, J., Saynisch, J., Schnepf, N.R., 2019. Modelling of electromagnetic signatures of global ocean circulation: physical approximations and numerical issues. Earth Planets Space, 71(1), 58. https://doi.org/10.1186/s40623-019-1033-7

[18] Khalilabadi, M.R. 2022. Underwater Terrain and Gravity aided inertial navigation based on

Kalman filter. International Journal of Coastal and Offshore Engineering, 5(3), 15-21.

[19] Kuvshinov, A. V., 2008. 3-D global induction in the oceans and solid Earth: recent progress in modeling magnetic and electric fields from sources of magnetospheric, ionospheric and oceanic origin. Surveys in Geophysics, Vol, 29, no, 2, pp. 139-186. https://doi.org/10.1007/s10712-008-9045-z

[20] Thébault, E., Finlay, C.C., Beggan, C.D., Alken, P., Aubert, J., Barrois, O., Bertrand, F., Bondar, T., Boness, A., Brocco, L., Canet, E., Chambodut, A., Chulliat, A., Coïsson, P., Civet, F., Du, A., Fournier, A., Fratter, I., Gillet, N., Hamilton, B., Hamoudi, M., Hulot, G., Jager, T., Korte, M., Kuang, W., Lalanne, X., Langlais, B., Léger, J.-M., Lesur, V., Lowes, F. J., Macmillan, S., Mandea, M., Manoj, C., Maus, S., Olsen, N., Petrov, V., Ridley, V., Rother, M., Sabaka, T. J., Saturnino, D., Schachtschneider, R., Sirol, O., Tangborn, A., Thomson, A., Tøffner-Clausen, L., Vigneron, P., Wardinski, I., and Zvereva, T., 2015. International Geomagnetic Reference Field: the 12th generation. Earth Planets Space, vol, 67, no, 1, pp. 79.

[21] Dostal, J., 2014. Modelling of the magnetic field induced by ocean circulation, Doctoral dissertation, Institut f¨ur Meteorologie Freie Universit¨at Berlin.

[22] Mandea, M., Thébault, E., 2007. The changing faces of the Earth's magnetic field: a glance at the magnetic lithospheric field, from local and regional scales to a planetary view. Published by Commission for the Geological Map of the World.

[23] Key, K., Constable, S., 2011. Coast effect distortion of marine magnetotelluric data: Insights from a pilot study offshore northeastern Japan. Physics of the Earth & Planetary Interiors, Vol, 184, no, 3-4, pp. 194-207.

[24] Fedorov, K., 2002. Formulas for converting the electrical conductivity of sea water into salinity with a digital temperature-salinity probe under average ocean conditions. Oceanology, 11(4), pp. 622-626.

[25] Apel, J. R., 1987. Principles of Ocean Physics, International Geophysics Series, Academic Press, San Diego, California, Vol. 38.

[26] Irrgang, C., Saynisch, J., Thomas, M., 2016. Impact of variable sea-water conductivity on motional induction simulated with an OGCM. Ocean Science Discussions, Vol, 12, no, 4, pp. 1869-1891.

[27] Thomas, M., Saynisch, J., Irrgang, C., 2016. Impact of variable sea-water conductivity on motional induction simulated with an OGCM. Ocean Science Discussions, Vol, 12, no, 4, pp. 1869-1891.

[28] Lilley, F.E., White, A., and Heinson, G.S., 2001. Earth's magnetic field: Ocean contributions to vertical profiles in deep oceans, Geophys. J. Int., 147, 163 – 175.

[29] Glazman, R. E., Golubev, Y. N, 2005. Variability of the ocean-induced magnetic field predicted at sea surface and at satellite altitudes. Journal of Geophysical Research: Oceans, Vol, 110, no, C12.

[30] Saynisch, J., Petereit, J., Irrgang, C., Kuvshinov, A., Tomas, M., 2016. Impact of climate variability on the tidal oceanic magnetic signal-A model based sensitivity study. Journal of Geophysical Research Oceans, Vol, 121, no, 8, pp. 5931-5941.

[31] Kuvshinov, A., Sabaka, T., and Olsen, N., 2006. 3-D electromagnetic induction studies using the Swarm constellation: Mapping conductivity anomalies in the Earth's mantle, Earth Planets Space, 58, 417– 427.

[32] Kuvshinov, A., and Utada, H., 2010. Anomaly of the geomagnetic Sq variation in Japan: effect from 3-D subterranean structure or the ocean effect? Geophys. J. Int. 183, 1239–1247.

[33] Schnepf, N. R., Kuvshinov, A., and Sabaka, T., 2015. Can we probe the conductivity of the lithosphere and upper mantle using satellite tidal magnetic signals? Geophys. Res. Lett., 42, 3233–3239, https://doi.org/10.1002/2015GL063540.

[34] Rabinovich, A.B., and Eblé, M.C., 2015. Deep-Ocean Measurements of Tsunami Waves. Pure Appl. Geophys. 172, 3281–3312 (2015). https://doi.org/10.1007/s00024-015-1058-1

[35] Dordipour, I., Ghadiri, H., Bybordi, M., Siadat, H., Malakouti, M. J., Hussein, J. 2004. The use of saline water from the Caspian Sea for irrigation and barley production in northern Iran. 13th International Soil Conservation Organisation Conference – Brisbane.

[36] Lebedev, S., 2018. Climatic variability of water circulation in the Caspian Sea based on satellite altimetry data. International journal of remote sensing, Vol, 39, no, 13, pp. 4343-4359.

[37] Ibrayev, R.A., Özsoy, E., Schrum, C., and Sur, H.I., 2010. Seasonal variability of the Caspian Sea three-dimensional circulation, sea level and air-sea interaction, Ocean Sci, *6*(1), 311-329. https://doi.org/10.5194/os-6-311-2010

[38] Zereshkian, S., and Mansoury, D., 2018. Evaluation of Offshore Wind Power to Supply the Electric Power Required for Offshore Oil and Gas Platforms in the Caspian Sea, Journal, of Hydrophysics, 4(1): 57-68.

[39] Zereshkian, S., and Mansoury, D., 2020. Evaluation of ocean thermal energy for supplying the electric power of offshore oil and gas platforms, Journal of the Earth and Space Physics,

Vol. 46, No. 2, 331-345. https://doi.org/10.22059/jesphys.2020.289441.1007161

[40] Baidin, S.S., Kosarev, A.N., 1986. The Caspian Sea. Hydrology and hydrochemistry, Moscow, Nauka, 261 pp (in Russian)

[41] Safari, M., Mansoury, D., & azarmsa, S. A. (2022). Grain-size characteristics of seafloor sediment and transport pattern in the Caspian Sea (Nowshahr and Babolsar coasts). International Journal of Coastal and Offshore Engineering, *7*(1), 34-42.

[42] Blumberg, A.F., and Mellor, G.L., 1987. A description of a three-dimensional coastal ocean circulation model. Three-Dimensional Coastal Ocean Models, Vol. 208, Heaps, N.S. (Ed.), American Geophysical Union, https://doi.org/10.1029/CO004p0001

[43] Mellor, G.L., Yamada, T., 1982. Development of a turbulence closure submodel for geophysical fluid problems. Rev. Geophys. Space Phys. 20, 851–875. https://doi.org/10.1029/RG020i004p00851

[44] Smagorinsky, J., 1993. In: Galperin, B., Orszag, S. (Eds.), 1993. Large Eddy Simulations of Complex Engineering and Geophysical Flows, Cambridge University Press.

[45] Korotenko, K., Mamedov, R., Kontar, A., and Korotenko, L., 2004. Particle tracking method in the approach for prediction of oil slick transport in the sea: modelling oil pollution resulting from river input, Journal of Marine Systems, vol. 48, p.159-170.

[46] Cherkesov, L.V., Shul'ga, T.Ya., 2018. Numerical Analysis of the Effect of Active Wind Speed and Direction on Circulation of Sea of Azov Water with and without Allowance for the Water Exchange through the Kerch Strait. Oceanology, 58, 19–27. DOI:10.1134/S0001437018010022

[47] Medvedev, I.P., Kulikov, E.A., and Fine, I.V., 2020. Numerical modelling of the Caspian Sea tides, Ocean Sci., 16, 209–219, https://doi.org/10.5194/os-16-209-2020.

[48] Oey, L., Chang, Y. L., Lin, Y. C., Chang, M. C., Xu, F., & Lu, H. F., 2013. ATOP-The Advanced Taiwan Ocean Prediction System Based on the mpiPOM. Part 1: Model Descriptions, Analyses and Results. *Terrestrial, Atmospheric & Oceanic Sciences*, *24*(1).

[49] Madala, R. V., and Piacsek, S. A., 1977. A semi-implicit numerical model for baroclinic oceans, J. Comput. Phys., 23, 167-178.

[50] Mellor, G. L., 1998. Users guide for a three-dimensional, primitive equation, numerical ocean model. Princeton, NJ: Program in Atmospheric and Oceanic Sciences, Princeton University.

[51] Kara A.B., Wallcraft A.J., Metzger E.J., Gunduz M., 2010. Impacts of freshwater on the seasonal variations of surface salinity and circulation in the Caspian Sea. Continental Self Research, 30(10):1211-25.

[52] UNESCO-IHP-IOC-IAEA, 1996. Workshop on sea level rise and multidisciplinary studies of environmental processes in the Caspian region 9-12 May. Paris, Farance IOC workshop No 108.

[53] Mansoury, M., Sadri Nasab, M., and Akbari Nasab, M., 2015. Modeling of salinity and temperature field structure in the Caspian Sea using POM model, Hydrophysics, 1(1), pp. 1-13. (Persian)

[54] Maus, S. Macmillan, S., Chernova, T., Choi, S., Dater, D., Golovkov, V., Lesur, V., Lowes, F., Lühr, H., Mai, W., Mclean, S., Oslen, N., Rother, M., Sabaka, T., Thomson, A., Zvereva, T., 2005. The 10th-Generation International Geomagnetic Reference Field, Geophys. J. Int., 161, 561–565. https://doi.org/10.1111/j.1365-246X.2005.02641.x

[55] Maus, S., Manoj, C., Rauberg, J., Michaelis, I., and Lühr, H, 2010. NOAA/NGDC candidate models for the 11th generation International Geomagnetic Reference Field and the concurrent release of the 6th generation Pomme magnetic model, Earth Planets Space, 62 (2). https://doi.org/10.5047/eps.2010.07.006

[56] Macmillan, S., and Finlay, C., 2010. The International Geomagnetic Reference Field. In: Mandea, M., Korte, M., (eds) Geomagnetic Observations and Model. IAGA Special Sopron Book Series, vol 5. Springer, Dordrecht. https://doi.org/10.1007/978-90-481-9858-0_10

[57] Finlay, C.C., Maus, S., Beggan, C.D., Bondar, T.N., Chambodut, A., Chernova, T.A., Chulliat, A., Golovkov, V.P., Hamilton, B., Hamoudi, M., Holme, R., Hulot, G., Kuang, W., Langlais, B., Lesur, V., Lowes, F. J., Luhr, H., Macmillan, S., Mandea, M., Michaelis, I., Olsen, N., Rauberg, J., Rother, M., Sabaka, T. J., Tangborn, A., Tøffner-Clausen, L., Thebault, E., Thomson, A. W. P., Wardinski, I., Zvereva, T. I, 2010. International geomagnetic reference field: the eleventh generation. Geophysical Journal International, Vol, 183, no, 3, pp. 1216-1230. https://doi.org/10.1111/j.1365-246X.2010.04804.x